Journal of Materials Chemistry C

COMMUNICATION

View Article Online
View Journal | View Issue

Cite this: J. Mater. Chem. C, 2014, 2, 3521

Received 7th November 2013
Accepted 5th March 2014

DOI: 10.1039/c3tc32191f

www.rsc.org/MaterialsC

Panchromatic light harvesting by N719 with a porphyrin molecule for high-performance dye-sensitized solar cells†

Shuai Chang,‡[a] Hongda Wang,‡[b] Lawrence Tien Lin Lee,[a] Shizhao Zheng,[a] Quan Li,[a] King Young Wong,[a] Wai-Kwok Wong,[b] Xunjin Zhu,*[b] Wai-Yeung Wong,*[b] Xudong Xiao*[a] and Tao Chen*[a]

We report efficient panchromatic light harvesting by co-adsorption of a porphyrin molecule and N719 in dye-sensitized solar cells. The co-sensitized device shows a considerably enhanced power conversion efficiency of 8.89%, while those individually sensitized by porphyrin and N719 display efficiencies of 7.21% and 8.02%, respectively. The porphyrin-sensitized device shows strong photocurrent generation in the Soret and Q bands, while N719 shows efficient spectral response in the 500–600 nm range; the combination of these two kinds of dye molecules displays a strong spectral response in the full-colour region. Mechanistic investigations are carried out by various spectral and electrochemical characterizations.

Introduction

Dye-sensitized solar cells (DSSCs) have attracted increasing interest in recent years due to the economical and ecological device fabrication and reasonably high power conversion efficiency (PCE, η).[1,2] In such device structures, a dye sensitizer harvests sunlight and injects electrons into the conduction band of a semiconducting oxide; the dye is then regenerated through a redox reaction. During the past decade, tremendous effort has been made to optimize every single component of the DSSCs,[3–7] which in turn provide a lot of practical and fundamental insight into device operation.[8–10] It has been realized that the light harvesting efficiency plays a key role in determining the final PCE.

One approach to extend the light response is to develop new dye molecules to cover a broad solar spectrum. Because the design of new dye molecules requires intricate play between the narrowing of the energy gap of the dye molecules, efficient charge injection and the dye regeneration limit, this sets a barrier for the design of dye molecules. Furthermore, though the design of molecules can be performed with theoretical prediction, the practical synthesis is not necessarily achievable. This is probably one of the most important reasons why the improvement of the energy conversion efficiency in DSSCs has not been that rapid. In dye molecule development, there are several classes of molecules possessing strong light responses in their respective regions. Therefore, an alternative approach to improve the light harvesting by a device would be sensitizing the device using multiple, complementary dye molecules to achieve a broad range light response.[9,11–18] In addition, other methods such as the use of energy relay dye molecules or plasmonic metal nanoparticles can also enhance light harvesting in DSSCs.[19,20]

In this work, we developed a push–pull porphyrin dye (denoted as HD18) and co-sensitized it with the state-of-the-art N719 dye molecules for the enhancement of the spectral response. Typically, porphyrin-based dyes possess high extinction coefficients in the Soret (400–500 nm) and Q (600–700 nm) absorption bands; hence, sunlight with wavelengths in these ranges could be completely harvested in optimized device structures.[1,21,22] However, one disadvantage of porphyrin dyes is that they have a relatively small absorption coefficient in the region between the two bands (500–600 nm), while the solar spectrum possesses a major portion of light in this region. This spectral characteristic sets a photovoltaic energy conversion limit in porphyrin-sensitized solar cells. On the other hand, the state-of-the-art ruthenium-based dyes (*e.g.* N719) exhibit excellent photovoltaic properties and display strikingly strong absorption in the 500–600 nm region, while the spectral response decreases quickly at longer wavelengths as well as in the blue region.[2] Therefore, a combination of the two types of dye molecules will be an effective way to improve the overall light harvesting in DSSCs.

[a]Department of Physics, The Chinese University of Hong Kong, Shatin, Hong Kong, China. E-mail: taochen@phy.cuhk.edu.hk; xdxiao@phy.cuhk.edu.hk; Fax: +852-2603 5204; Tel: +852-3943 6278

[b]Institute of Molecular Functional Materials, Department of Chemistry and Institute of Advanced Materials, Hong Kong Baptist University, Waterloo Road, Kowloon Tong, Hong Kong, China. E-mail: rwywong@hkbu.edu.hk; xjzhu@hkbu.edu.hk; Fax: +852-3411 7048; Tel: +852-3411 5157

† Electronic supplementary information (ESI) available. See DOI: 10.1039/c3tc32191f

‡ The authors contributed equally to the work.

Results and discussion

The synthetic route to HD18 is sketched in Scheme 1. The detailed protocol is described in the Experimental section. Nuclear magnetic resonance (NMR) and high-resolution mass spectrometry (HRMS) characterizations of the as-synthesized porphyrin molecule are provided in Fig. S1 and S2,† which confirm the structure of HD18 in Scheme 1. In the use of porphyrin to sensitize a TiO_2 nanoparticle film, it is generally observed that porphyrin molecules tend to aggregate on the surface, which usually lead to self-quenching and reduce the efficiency of electron injection into TiO_2.[23–25] Therefore, engineering of porphyrin sensitizers with enhanced stability and inhibition of aggregation is paramount. In this study, the push–pull zinc porphyrin HD18 based on the *ortho*-alkylated phenyl-substituted porphyrin core, in which the nonplanar (4-(bis(9,9-dimethyl-9*H*-fluoren-2-yl)amino)phenyl)ethynyl moiety serves as donor group,[26] can not only suppress aggregate formation but also increase the molar extinction coefficient of the organic sensitizer. In addition, the introduction of ethynylbenzoic acid in HD18 as an acceptor group can facilitate charge injection.

The electrochemical properties of HD18 were studied using cyclic voltammetry (CV) (Fig. 1). The measurement shows an oxidation potential of 0.62 V (*vs.* NHE), which corresponds to the highest occupied molecular orbital (HOMO) energy of the dye.[27] This value is more positive than the redox couple I^-/I_3^- (0.45 V *vs.* NHE), thus favorable kinetics for dye regeneration can be achieved. On the other hand, the lowest unoccupied molecular orbital (LUMO) was calculated to be −1.12 V (*vs.* NHE), which is higher than the conduction band of TiO_2 and thus enables efficient charge injection kinetics.

HD18 shows typical absorption peaks associated with Soret and Q bands, located at ~455 nm and ~665 nm (Fig. 2a),[17,21] with absorption coefficients of $1.67 \times 10^5\ M^{-1}\ cm^{-1}$ and $0.47 \times 10^5\ M^{-1}\ cm^{-1}$, respectively. The absorption features of HD18 anchoring onto TiO_2 film are similar to those in solution

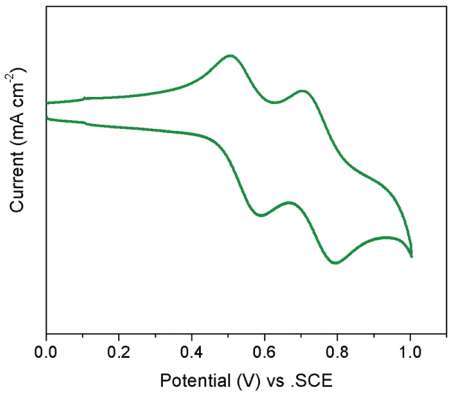

Fig. 1 Cyclic voltammetry scanning of the HD18.

(Fig. 2b). Obviously, these two light absorption bands are complementary to the state-of-the-art N719 dye molecule, which has strong absorption in the range of 500–600 nm (Fig. 2b). When the two types of dye are co-adsorbed onto the TiO_2 film, the light absorption shows an impressive enhancement when compared with each of the individually sensitized solar cells (Fig. 2b). Therefore, the combination of N719 dye molecules and a porphyrin-based sensitizer can offer a platform for strong panchromatic sunlight harvesting.

DSSCs were fabricated according to our reported method with modifications.[20,28,29] The fabrication of a co-sensitized anode was performed by sequential soaking of the anode film in dye solutions. For comparison, DSSCs individually sensitized by HD18 (device **1**) and N719 (device **2**) were also prepared. Optimizations showed that TiO_2 films with their anodes consisting of a 12 μm transparent layer and a 6 μm scattering TiO_2 layer, immersed in porphyrin dye for 12 h, followed by adsorbing N719 for 3 h, give rise to the highest PCE (8.89% ± 0.06%) of the co-sensitized device (device **3**, Fig. 3, the device parameters are tabulated in Table 1). At the same time, devices **1** and **2** show

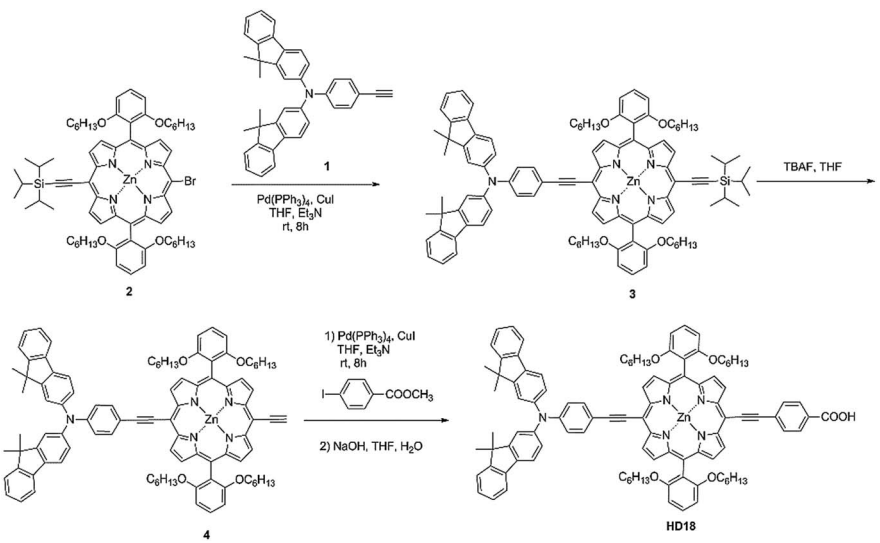

Scheme 1 Synthetic route for HD18.

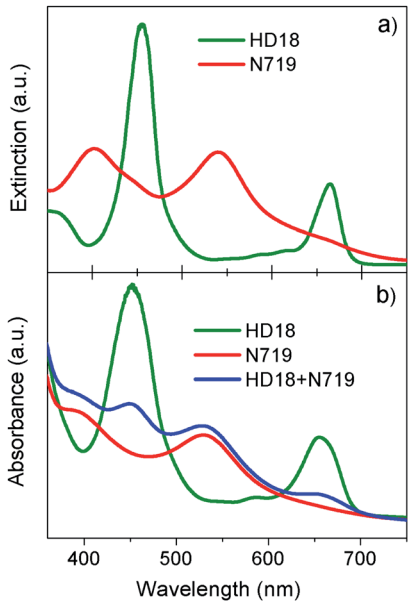

Fig. 2 (a) UV-vis absorption of HD18 and N719 in THF solution and (b) HD18, N719, and HD18 and N719 co-adsorbed on TiO_2 films (thickness 3).

PCEs of 7.21% and 8.02%, with short-circuit photocurrent densities (J_{sc}) of 15.48 and 16.47 mA cm^{-2}, respectively. It should be noted that, to make fair comparisons, the dye loading times for devices **1** and **2** are 16 h, and these are optimized durations for the corresponding dye molecules.

To elucidate the improved J_{sc} in the co-sensitized device, we performed incident photon-to-electron conversion efficiency (IPCE) characterization. The IPCE is associated with the product of light harvesting efficiency (η_{lh}), charge injection efficiency (η_{inj}), and charge collection efficiency (η_{coll}).[2] From Fig. 4, the IPCE of device **3** is boosted in a broad spectrum and exhibits two humps from 400–500 nm and 600–700 nm when compared with the DSSC individually sensitized by N719. These two bands correspond to the strong absorption of HD18. On the other hand, compared with the DSSCs sensitized by HD18, the photocurrent generation in the 500–600 nm range is greatly enhanced. Therefore, the co-sensitized device can take advantage of both types of dye molecules. The significantly improved J_{sc} in device **3** (18.51 ± 0.08 mA cm^{-2}) is thus mainly due to the improved light harvesting, which is consistent with the UV-visible spectra alternations where the co-sensitized film presents increased light absorption.

Table 1 J_{sc}, V_{oc}, fill factor (FF) and PCE (η) parameters of devices **1**–**3** measured under one sun (AM 1.5 G) illumination

Device[a]	J_{sc} (mA cm^{-2})	V_{oc} (V)	FF (%)	η (%)
1	15.48	0.693	67.2	7.21
2	16.47	0.732	66.5	8.02
3[b]	18.51	0.711	67.7	8.89

[a] The effective areas of all the devices are 0.24 cm^2. [b] The data of device **3** is an average of three identical devices; details are provided in Fig. S4.

The open-circuit voltage (V_{oc}) of the co-sensitized device **3** (0.711 ± 0.002) falls in between those of the devices sensitized solely with HD18 (0.693 V) and N719 (0.732 V); such a phenomenon is commonly seen in a co-sensitizing configuration. To gain insight into the co-sensitizing mechanism, we performed electrochemical impedance spectroscopy (EIS) under dark conditions. As shown in Fig. 5a, the *x*-intercepts of the EIS curves indicate the resistance of the fluorine-doped tin oxide (FTO) glass surface. The straight lines at high frequencies imply ion diffusion resistance through the 3D anode network. They are overlapped, indicating similar ion transport speed in the devices. Further, the Nyquist arcs appearing at the intermediate-frequency regime are associated with the recombination resistance (R_{ct}) at the interface of TiO_2/dye/electrolyte, *i.e.*, the recombination kinetics between conduction-band electrons in TiO_2 and I_3^- species from the electrolyte. The calculated resistance values (R_{ct}) are listed in Table S1;† the larger the R_{ct}, the slower the recombination kinetics. It is noted that device **2** presents the largest R_{ct} (196.4 Ω, Table S2†). Slower recombination would lead to higher V_{oc}. Therefore, device **2** shows high

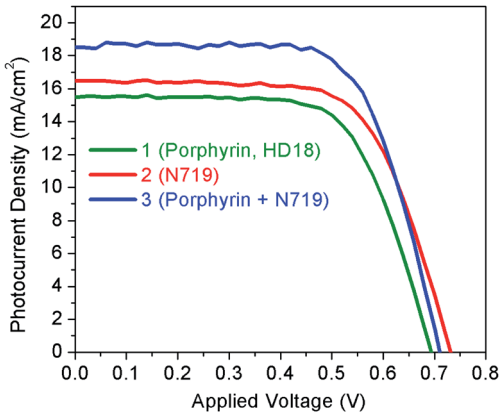

Fig. 3 (a) Photocurrent–voltage (*J*–*V*) characteristics of devices sensitized by HD18, N719 and HD18 + N719.

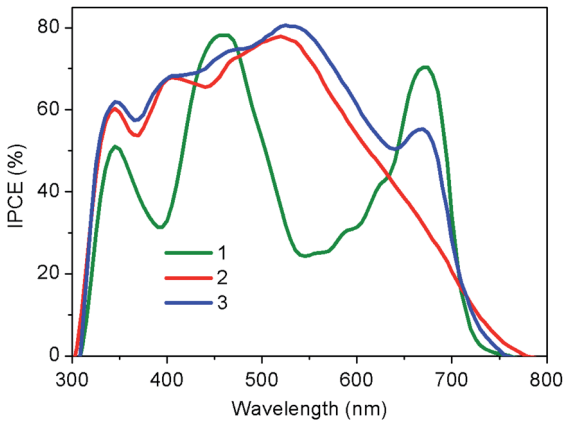

Fig. 4 Incident photon-to-electron conversion efficiency (IPCE) spectra of devices sensitized by HD18 (device **1**), N719 (device **2**) and HD18 + N719 (device **3**).

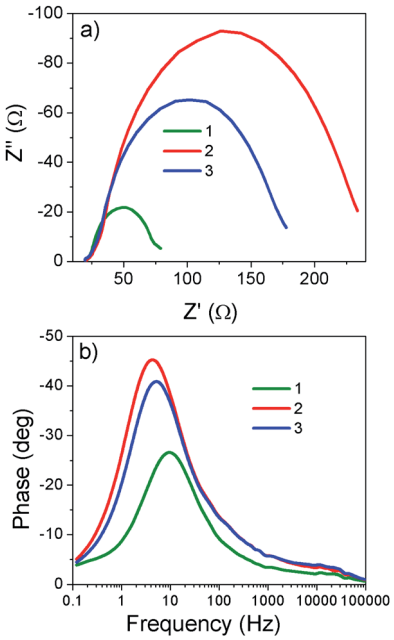

Fig. 5 (a) Nyquist and (b) Bode phase plots of DSSCs based on individual HD18 and N719 electrode (devices **1** and **2**) and HD18 + N719 co-sensitized electrodes (device **3**).

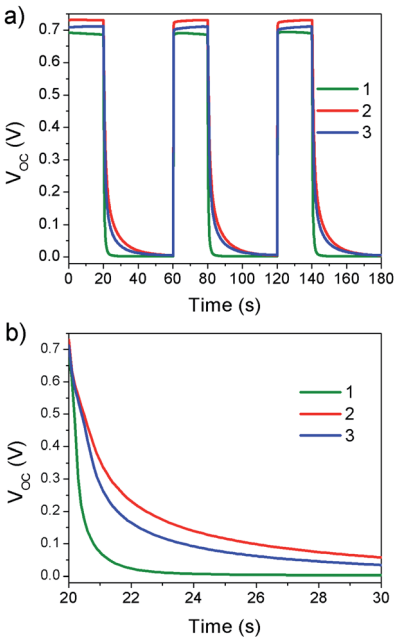

Fig. 6 (a) Open-circuit voltage decay profiles of devices **1**–**3** and (b) enlarged profiles in the interval from 20 to 30 seconds.

V_{oc}. The lowest V_{oc} of the HD18 sensitized device is associated with the smallest R_{ct} (52.2 Ω). Furthermore, the calculated R_{ct} of co-sensitized device **3** is 142.1 Ω, which is in between those of devices **1** and **2**. This observation is consistent with V_{oc} evolution as discussed above.

From the Bode phase plots of the devices (Fig. 5b), the characteristic back charge transfer frequency (f) can be obtained, which corresponds to the peak of the Bode phase plot. The electron lifetime (τ_n) in the TiO_2 film can be calculated from eqn (1):[30,31]

$$\tau_n = \frac{1}{2\pi f} \quad (1)$$

where f is the characteristic frequency, corresponding to the peak in the intermediate-frequency regime. The obtained τ_n values are also shown in Table S1.† It can be seen that the device sensitized by HD18 alone displays the shortest τ_n among all the devices. In the device with the co-adsorption of N719, the electron lifetime is prolonged to a value quite close to that of the device sensitized with N719 alone.

To further probe the recombination kinetics of the devices, open-circuit voltage decay (OCVD) curves were recorded, which can continuously record the lifetime of V_{oc} from a steady state to dark equilibrium.[32] Fig. 6a shows the OCVD profiles of devices **1** to **3**. The profiles at the interval of 20 to 30 seconds were enlarged for clearer observation (Fig. 6b). The correlation between V_{oc} decay and electron lifetime (τ_n) can be expressed by eqn (2):

$$\tau_n = -\frac{K_B T}{e}\left(\frac{dV_{oc}}{dt}\right)^{-1} \quad (2)$$

where K_B is the Boltzmann constant, T is temperature, and e is the electron charge.[8,32] Therefore, the electron lifetimes can be extracted from the initial slope of V_{oc} decay curves. First, the decay curve of device **1** presents the steepest slope while that of device **2** displays the slowest one, which suggests the shortest electron lifespan is for the HD18-sensitized device and the longest one is for the N719-sensitized device. This variation matches well with the photovoltaic and EIS analyses of the devices made by the two dyes.

Conclusions

We have demonstrated for the first time panchromatic light harvesting by the co-sensitization of a porphyrin-based dye and N719 in dye-sensitized solar cells. Remarkable improvements of 23.3% and 10.8% are achieved in the co-sensitized devices when compared with the devices individually sensitized by HD18 and N719, respectively. Generally, porphyrin-based dyes possess a spectral response complementary to that of ruthenium-complex based dyes. This type of co-sensitization is anticipated to arouse broad interest in further boosting the efficiency of dye-sensitized solar cells by using these two important classes of molecules.

Experimental

Materials

All chemical reagents were used without further purification.

Dye sensitizer *cis*-bis(isothiocyanato)bis(2,2′-bipyridyl-4,4′-dicarboxylato)-ruthenium(II)-bis-tetrabutylammonium, (coded as N719), TiO_2 paste (DSL 18NR-T) and iodide-based liquid electrolyte (HL-HPE) were purchased from Dyesol company. Compounds

N-(9,9-dimethyl-9*H*-fluoren-3-yl)-*N*-(4-ethynylphenyl)-9,9-dimethyl-9*H*-fluoren-2-amine **1** (ref. 33) and **2** (ref. 34) were prepared according to the literature.

3: To a 50 mL, two-necked round-bottom flask, compound **2** (237 mg, 0.2 mmol), **1** (301 mg, 0.6 mmol), anhydrous THF (10 mL), and triethylamine (5 mL) were added. The mixture was deoxygenated with N_2 for 30 min. Then $Pd(PPh_3)_4$ (48 mg, 0.04 mmol) and CuI (8 mg, 0.04 mmol) were added. The mixture was stirred at room temperature for 8 h. The solvent was removed, and the residue was purified by chromatography on silica gel with CH_2Cl_2–hexane (1 : 1, v/v) to give **3** as a green solid (273 mg, yield 85%).

4: To a solution of **3** (32.1 mg, 20.0 μmol) in 5 mL of dry THF, 1 M TBAF in THF (80 μL, 80 μmol) was added by syringe. The mixture was stirred at room temperature in the dark under argon for 45 min and quenched with de-ionized water. The mixture was extracted with CH_2Cl_2 twice, and the organic layers were collected and dried with anhydrous Na_2SO_4. After removal of the solvents, the crude product **4** was used without further purification in the next step.

Porphyrin dye (HD18). To a 50 mL, two-necked round-bottom flask, compound **4** (20 mg, 13.8 μmol), methyl 4-iodobenzoate (36 mg, 138 μmol), anhydrous THF (5 mL), and triethylamine (2 mL) were added. The mixture was deoxygenated with N_2 for 10 min, then $Pd(PPh_3)_4$ (4.8 mg, 4.0 μmol) and CuI (0.8 mg, 4.0 μmol) were added to the mixture. The resultant mixture was stirred at room temperature for 8 h. The reaction mixture was extracted with CH_2Cl_2 and washed twice with water. The organic layer was collected and dried over anhydrous Na_2SO_4. The solvent was then removed, and the residue was purified on a silica gel column eluted with CH_2Cl_2–hexane (1 : 1, v/v) to give the methyl ester-protected porphyrin dye. The crude product was further dissolved in 4 mL of THF and 1 mL of methanol, then 1 mL of 1 M NaOH aqueous solution was added by syringe. The solution was refluxed under argon for 2 h and cooled to room temperature. The pH value was adjusted to around 4 by adding 1 M HCl. The mixture was extracted with $CHCl_3$ twice, and the organic layer collected was dried with anhydrous Na_2SO_4. After removal of the solvent, the crude product was purified on a silica gel column eluted with $CHCl_3$–CH_3OH (15/1 v/v) and recrystallized from methanol–$CHCl_3$ to give the target porphyrin dye as a green powder (19.5 mg, 90%). ^{1}H NMR (400 MHz, $CDCl_3$) δ (ppm): 0.18–0.20 (m, 12H, CH_3 H), 0.38–0.49 (m, 24H), 0.90–1.00 (m, 8H), 1.38 (s, 12H, CH_3 H), 3.80–3.82 (t, 8H), 6.94–6.97 (m, 4H), 7.11–7.28 (m, 12H), 7.33–7.35 (d, J = 2.0 Hz, 2H), 7.58–7.67 (m, 8H), 7.90 (d, J = 2.0 Hz, 2H), 8.76 (d, J = 4.4 Hz, 2H, β-pyrrolic H), 8.80 (d, J = 4.4 Hz, 2H, β-pyrrolic H), 9.44(d, J = 4.4 Hz, 2H, β-pyrrolic H), 9.49 (d, J = 4.4 Hz, 2H, β-pyrrolic H). MS (MALDI-TOF, m/z) calculated for $C_{103}H_{101}N_5O_6Zn$: 1570.3213; found: 1570.3264%.

Device fabrication

A layer of ~6 μm TiO_2 paste (particle size ~20 nm) was doctor-bladed onto FTO conducting glass and then dried for 6 min at 150 °C. This procedure was repeated to prepare a thickness of ~12 μm, and the resulting surface was finally coated by a scattering layer (~6 μm) of TiO_2 paste (particle size ~200 nm). The final thickness of the electrodes is ~18 μm. These TiO_2 electrodes were gradually heated under an air flow at 275 °C for 5 min, 325 °C for 5 min, 375 °C for 5 min, and 470 °C for 30 min to remove polymers. Then, these sintered films were soaked with 0.02 M TiF_4 aqueous solution for 60 min at 70 °C, washed with deionized water, and further annealed at 450 °C for 30 min. For dye loading, the electrodes were first immersed into a 0.2 mM HD18 dye bath (acetonitrile–*tert*-butyl alcohol (1 : 1, v/v) solution, with 10 mM chenodeoxycholic acid (CDCA)) for 12 h. Afterwards, the electrodes were transferred into a 0.5 mM N719 dye bath in acetonitrile–*tert*-butyl alcohol (1 : 1, v/v) solution for 3 h. The electrodes were then rinsed with ethanol to remove the non-adsorbed dyes and dried in air. In addition, the dye soaking times for the anodes of device **1** and **2** are 16 h, which are the standard time spans. Finally, the dye soaked films were stacked with a Pt-based counter electrode and filled with iodine/iodide-based electrolyte. The effective areas of all the devices were 0.24 cm^2.

Material and device characterizations

NMR spectra were recorded on a Bruker Ultrashield 400 Plus NMR spectrometer. High resolution mass spectrometry (HRMS) was performed on a Bruker Autoflex MALDI-TOF mass spectrometer. UV-vis absorption spectra were obtained using a Hitachi U-3501 UV-visible/NIR spectrophotometer. The current density–voltage (J–V) characteristics of the assembled cells were measured by a semiconductor characterization system (Keithley 236) at room temperature in air under the spectral output from a solar simulator (Newport) using an AM 1.5 G filter with a light power of 100 mW cm^{-2}. Electrochemical impedance spectroscopy (EIS) was performed by applying a bias of 700 mV under dark conditions over a frequency range of 0.1–10^5 Hz with an AC amplitude of 10 mV, and the parameters were calculated from Z-View software (v2.1b, Scribner AssociatNe, Inc.). For the open-circuit voltage decay measurements, the cell was first illuminated for 20 s to a steady voltage, then the illumination was turned off for 40 s and the photovoltage decay curve was recorded; this process was repeated for three periods to further confirm the stability of the cell. The above two measurements were performed on a CHI 660D electrochemical workstation. The photocurrent conversion efficiency spectra of DSSCs were recorded using a Solar Cell QE/IPCE measurement system (Zolix Solar Cell Scan 100) in DC mode.

Acknowledgements

The authors acknowledge the financial support from the CUHK Group Research Scheme, CUHK Focused Scheme B Grant "Center for Solar Energy Research" and the university research grant (code: 4053068). X. Zhu thanks the financial support from Hong Kong Baptist University (Grants FRG2/12-13/050 and FRG1/13-14/022). W. K. W. and W. Y. W. are grateful for a grant from the Areas of Excellence Scheme, University Grants Committee, Hong Kong (project no. [AoE/P-03/08]). W. Y. W. also thanks Hong Kong Research Grants Council (HKBU203011) and The Science,

Technology and Innovation Committee of Shenzhen Municipality (JCYJ20120829154440583) for financial support.

Notes and references

1 L. L. Li and E. W. G. Diau, *Chem. Soc. Rev.*, 2013, **42**, 291–304.
2 A. Hagfeldt, G. Boschloo, L. C. Sun, L. Kloo and H. Pettersson, *Chem. Rev.*, 2010, **110**, 6595–6663.
3 M. X. Wu, X. Lin, Y. D. Wang, L. Wang, W. Guo, D. D. Qu, X. J. Peng, A. Hagfeldt, M. Grätzel and T. L. Ma, *J. Am. Chem. Soc.*, 2012, **134**, 3419–3428.
4 Y. Bai, Y. M. Cao, J. Zhang, M. Wang, R. Z. Li, P. Wang, S. M. Zakeeruddin and M. Grätzel, *Nat. Mater.*, 2008, **7**, 626–630.
5 F. C. Krebs and M. Biancardo, *Sol. Energy Mater. Sol. Cells*, 2006, **90**, 142–165.
6 B. Liu, W. Q. Li, B. Wang, X. Y. Li, Q. B. Liu, Y. Naruta and W. H. Zhu, *J. Power Sources*, 2013, **234**, 139–146.
7 S. M. Wang, W. W. Dong, R. H. Tao, Z. H. Deng, J. Z. Shao, L. H. Hu, J. Zhu and X. D. Fang, *J. Power Sources*, 2013, **235**, 193–201.
8 J. Bisquert, A. Zaban, M. Greenshtein and I. Mora-Sero, *J. Am. Chem. Soc.*, 2004, **126**, 13550–13559.
9 J. N. Clifford, E. Palomares, K. Nazeeruddin, R. Thampi, M. Gratzel and J. R. Durrant, *J. Am. Chem. Soc.*, 2004, **126**, 5670–5671.
10 C. G. Zhang, J. Dai, Z. P. Huo, X. Pan, L. H. Hu, F. T. Kong, Y. Huang, Y. F. Sui, X. Q. Fang, K. J. Wang and S. Y. Dai, *Electrochim. Acta*, 2008, **53**, 5503–5508.
11 T. Bessho, S. M. Zakeeruddin, C. Y. Yeh, E. W. G. Diau and M. Grätzel, *Angew. Chem., Int. Ed.*, 2010, **49**, 6646–6649.
12 M. Kimura, H. Nomoto, N. Masaki and S. Mori, *Angew. Chem., Int. Ed.*, 2012, **51**, 4371–4374.
13 N. Robertson, *Angew. Chem., Int. Ed.*, 2008, **47**, 1012–1014.
14 J. H. Yum, S. R. Jang, P. Walter, T. Geiger, F. Nuesch, S. Kim, J. Ko, M. Gratzel and M. K. Nazeeruddin, *Chem. Commun.*, 2007, 4680–4682.
15 M. Mojiri-Foroushani, H. Dehghani and N. Salehi-Vanani, *Electrochim. Acta*, 2013, **92**, 315–322.
16 A. Yella, H. W. Lee, H. N. Tsao, C. Y. Yi, A. K. Chandiran, M. K. Nazeeruddin, E. W. G. Diau, C. Y. Yeh, S. M. Zakeeruddin and M. Gratzel, *Science*, 2011, **334**, 629–634.
17 S. Chang, H. Wang, Y. Hua, Q. Li, X. Xiao, W.-K. Wong, W. Y. Wong, X. Zhu and T. Chen, *J. Mater. Chem. A*, 2013, **1**, 11553–11558.
18 L. H. Nguyen, H. K. Mulmudi, D. Sabba, S. A. Kulkarni, S. K. Batabyal, K. Nonomura, M. Gratzel and S. G. Mhaisalkar, *Phys. Chem. Chem. Phys.*, 2012, **14**, 16182–16186.
19 J. H. Yum, B. E. Hardin, S. J. Moon, E. Baranoff, F. Nuesch, M. D. McGehee, M. Grätzel and M. K. Nazeeruddin, *Angew. Chem., Int. Ed.*, 2009, **48**, 9277–9280.
20 S. Chang, Q. Li, X. Xiao, K. Y. Wong and T. Chen, *Energy Environ. Sci.*, 2012, 9444–9448.
21 C. L. Wang, C. M. Lan, S. H. Hong, Y. F. Wang, T. Y. Pan, C. W. Chang, H. H. Kuo, M. Y. Kuo, E. W. G. Diau and C. Y. Lin, *Energy Environ. Sci.*, 2012, **5**, 6933–6940.
22 F. Gao, Y. Wang, D. Shi, J. Zhang, M. Wang, X. Jing, R. Humphry-Baker, P. Wang, S. M. Zakeeruddin and M. Grätzel, *J. Am. Chem. Soc.*, 2008, **130**, 10720–10728.
23 D. Liu, R. W. Fessenden, G. L. Hug and P. V. Kamat, *J. Phys. Chem. B*, 1997, **101**, 2583–2590.
24 I. Jung, J. K. Lee, K. H. Song, K. Song, S. O. Kang and J. Ko, *J. Org. Chem.*, 2007, **72**, 3652–3658.
25 S. Kim, H. Choi, D. Kim, K. Song, S. O. Kang and J. Ko, *Tetrahedron*, 2007, **63**, 9206–9212.
26 H. Choi, C. Baik, S. O. Kang, J. Ko, M. S. Kang, M. K. Nazeeruddin and M. Gratzel, *Angew. Chem., Int. Ed.*, 2008, **47**, 327–330.
27 C. L. Mai, W. K. Huang, H. P. Lu, C. W. Lee, C. L. Chiu, Y. R. Liang, E. W. G. Diau and C. Y. Yeh, *Chem. Commun.*, 2010, **46**, 809–811.
28 Y. Hua, S. Chang, D. D. Huang, X. Zhou, X. J. Zhu, J. Z. Zhao, T. Chen, W. Y. Wong and W. K. Wong, *Chem. Mater.*, 2013, **25**, 2146–2153.
29 T. Chen, W. Hu, J. Song, G. H. Guai and C. M. Li, *Adv. Funct. Mater.*, 2012, **22**, 5245–5250.
30 C. M. Li, C. Q. Sun, S. Song, V. E. Choong, G. Maracas and X. J. Zhang, *Front. Biosci.*, 2005, **10**, 180–186.
31 S. R. Sun, L. Gao and Y. Q. Liu, *Appl. Phys. Lett.*, 2010, **96**, 083113.
32 A. Zaban, M. Greenshtein and J. Bisquert, *ChemPhysChem*, 2003, **4**, 859–864.
33 Y. Shirota, M. Kinoshita, T. Noda, K. Okumoto and T. Ohara, *J. Am. Chem. Soc.*, 2000, **122**, 11021–11022.
34 T. G. Zhang, Y. X. Zhao, I. Asselberghs, A. Persoons, K. Clays and M. J. Therien, *J. Am. Chem. Soc.*, 2005, **127**, 9710–9720.

